

# Natural formation of bcc Co: Initial stage of Co precipitation in supersaturated Au<sub>90</sub>Co<sub>10</sub>

R. Bauer,<sup>1,\*</sup> E. Bischoff,<sup>2</sup> and E. J. Mittemeijer<sup>1,2</sup>

<sup>1</sup>*Institute for Materials Science, University of Stuttgart, Heisenbergstr. 3, 70569 Stuttgart, Germany*

<sup>2</sup>*Max Planck Institute for Metals Research, Heisenbergstr. 3, 70569 Stuttgart, Germany*

(Received 16 November 2009; revised manuscript received 17 February 2010; published 23 March 2010)

Natural formation of the bcc modification for Co was demonstrated to occur upon precipitation of Co in supersaturated Au<sub>90</sub>Co<sub>10</sub> alloy. The microstructural evolution was investigated by high-resolution transmission electron microscopy. Co precipitation starts with the formation of very thin coherent plates along {100}<sub>Au</sub>. This initially precipitated Co was shown to be a hitherto unknown metastable bcc modification of Co exhibiting a Bain-type orientation relationship with the matrix: (100)<sub>Au,fcc</sub>∥(100)<sub>Co,bcc</sub> and [001]<sub>Au,fcc</sub>∥[011]<sub>Co,bcc</sub> (three variants). Prolonged annealing causes the bcc Co to transform according to a Bain-type transformation into face-centered-cubic (fcc) Co, exhibiting the (cube-on-cube) orientation relationship (100)<sub>Au,fcc</sub>∥(100)<sub>Co,fcc</sub> and [001]<sub>Au,fcc</sub>∥[001]<sub>Co,fcc</sub> (three variants), in association with loss of coherency and a morphological change from Co platelets to equiaxed Co particles. A delicate balance of interface energy and bulk energy upon precipitation and subsequent growth/coarsening governs the successive appearance of the bcc and fcc modifications of Co.

DOI: [10.1103/PhysRevB.81.094113](https://doi.org/10.1103/PhysRevB.81.094113)

PACS number(s): 61.66.Dk, 64.70.K-, 68.37.Lp, 81.30.Mh

## I. INTRODUCTION

Au-Co alloys play an important role as contact material in microelectronic systems, as dental casting alloy and are also of interest as a material exhibiting giant magnetoresistance.<sup>1–3</sup> The until now known naturally occurring crystalline phases of cobalt have either the hexagonal-closed-packed (hcp) crystal structure, stable below 695 K (at 1 atm), and the face-centered-cubic (fcc) crystal structure, stable above 695 K (at 1 atm).<sup>4</sup> The investigation of the kinetics and microstructure changes and the underlying mechanisms of the allotropic hcp-fcc phase transformation in bulk and thin layer systems has been subject of research since decades.<sup>5–16</sup>

Artificially made thin layers of Co on a substrate can occur in a metastable (usually distorted) bcc modification likely as a consequence of prevailing very large strains in the concerned (multi) layer/substrate system.<sup>17–21</sup> The occurrence of pure bcc Co precipitates in the bulk of a supersaturated alloy upon precipitation has not been observed before.

This work provides the first experimental evidence of naturally occurring bcc Co precipitates in the early stage of precipitation in bulk Au<sub>90</sub>Co<sub>10</sub> alloy. The precipitation process was followed by differential scanning calorimetry (DSC) applying a step-by-step isochronal annealing treatment in combination with (high-resolution) transmission electron microscopy [(HR) TEM] at each step.

## II. EXPERIMENTAL

A cylindrical ingot of Au—10.12 at. % Co (further indicated as Au<sub>90</sub>Co<sub>10</sub>) with a diameter of 8 mm was produced by melting Au (99.95 at. %) and Co (99.995 at. %) in a protective argon atmosphere. The ingot was annealed in an evacuated silica capsule in a protective argon atmosphere (250 mbar at RT) and homogenized within a compensation body at 1233 K for 236 h. The ampoule was quenched in ice water by breaking the capsule. The ingot was hammered down to a diameter of 5 mm and subsequently cut into disks

of 500 μm thickness. The specimen disks were recrystallized at 1233 K for 24 h applying the same protective procedure as for the ingot, followed by quenching in ice water by breaking the capsules.

Isochronal annealing experiments were performed applying a DSC Pyris 1 from PerkinElmer. The DSC was calibrated using the temperature and enthalpy of melting of In, Pb, and Zn. Each specimen disk investigated was encapsulated in Al pans closed and sealed with an Al lid. As reference an empty Al pan with two lids was used to reach a heat capacity similar to that of the Al pan with the specimen. Isochronal annealing was performed with a heating rate of 20 K min<sup>−1</sup> starting from room temperature. Such DSC runs were interrupted at 550, 633, 668, and 773 K by fast cooling of the specimen at a rate of 180 K min<sup>−1</sup>. The Vickers micro hardness of the thus (partly) precipitated systems was measured using a microhardness tester LEICA VMHT MOT applying a load of 1 gf for 10 s. The microstructure of these specimens was investigated by (HR) TEM.

Specimens for (HR) TEM were prepared by cutting out a stripe from the disk, clamping and gluing it between two Al blades fixed by a Cu ring and cutting again a thin disk. After dimpling the disk to 100 μm, ion thinning was applied using a GATAN precision ion polishing system with a voltage of 3 kV, a current of 10 μA, an incident angle of 9° and a LN<sub>2</sub> cooling unit. TEM was performed using a Philips CM200 instrument operating at 200 kV, and HRTEM was performed using a JEOL 4000 FX instrument operating at 400 kV. The images and the selected-area electron-diffraction patterns were recorded with a charge-coupled-device camera. The composition of the Au matrix after completed precipitation (at 773 K) was determined by energy-dispersive x-ray (EDX) microanalysis in a VG501 scanning transmission electron microscopy (STEM) instrument.

## III. RESULTS

The baseline-corrected<sup>22</sup> isochronal DSC scan (heating rate of 20 K min<sup>−1</sup>) of an initially supersaturated Au<sub>90</sub>Co<sub>10</sub>

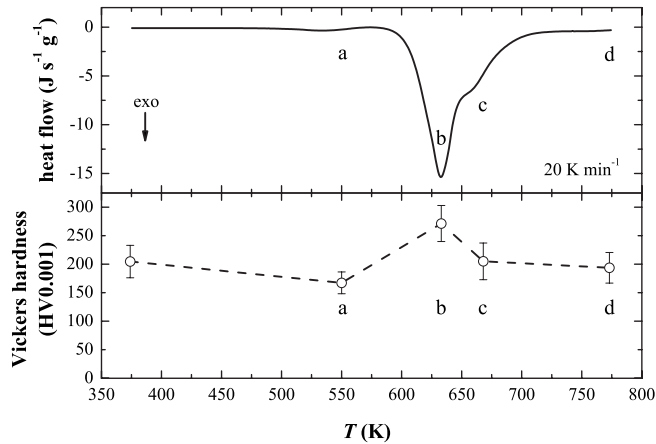


FIG. 1. Isochronal baseline-corrected DSC scan (heating rate of  $20 \text{ K min}^{-1}$ ) of initially supersaturated  $\text{Au}_{90}\text{Co}_{10}$  (top part of figure) and the corresponding hardness measurements [bottom part of figure; dashed line has been drawn to guide the eye; the experimental error in the hardness data (each data point is the average of 25 measurements) results from a 10% uncertainty in the determination of the diagonal length ( $2\text{--}5 \mu\text{m}$ ) of the indents]. a: relaxation of stresses due to quenching after homogenization/recrystallization (very weak exothermic preprecipitation peak and decrease in hardness); b: the formation of bcc Co precipitates takes place at temperatures higher than 580 K, leading to a distinct exothermic peak and an increase in hardness; c: the shoulder in the DSC scan at the high-temperature side of the strong exothermic peak is assigned to the bcc-to-fcc transformation of the Co precipitates in association with elastic (misfit) stress relaxation reaction (loss of coherency); and d: above 700 K only incoherent fcc Co particles occur within a Co-depleted Au matrix.

is shown in the top part of Fig. 1 together with the associated hardness changes in the bottom part of Fig. 1. The microstructure after quenching to room temperature exhibits a high number density of dislocations (as observed with TEM). No other structural defects (stacking faults, twins, “rodlike” defects) were found after intensive analysis. The very small exothermic preprecipitation peak “a” is due to the relaxation of quenched-in thermal stresses. At the same stage of isochronal annealing, a hardness decrease had occurred from  $205 \pm 28$  (as-quenched) to  $167 \pm 19$  HV (annealed to 550 K). The precipitation of Co starts at about 580 K leading to the second exothermic main peak (b+c). The exothermic main reaction consists of two parts: (i) a sharp, strong peak with a peak maximum at 633 K and a corresponding hardness increase to  $271 \pm 31$  HV (b) followed by (ii) a shoulder at higher temperatures around 668 K in combination with a hardness decrease to  $205 \pm 32$  HV (c). Similar observations were made using several fresh specimens applying heating rates in the range from 5 to  $40 \text{ K min}^{-1}$  (not shown here).

TEM bright-field and HRTEM images and corresponding selected-area diffraction patterns (SADPs) taken after isochronal annealing up to 633 K with  $20 \text{ K min}^{-1}$  [corresponding with exothermic peak maximum (Fig. 1 top) and hardness maximum (Fig. 1 bottom)], are shown in Fig. 2. Evidently very thin Co plates only 0.5–1 nm thick and with a lateral extension between 5 and 10 nm have developed. The habit plane of the precipitates is of  $\{100\}$  type: in case of a

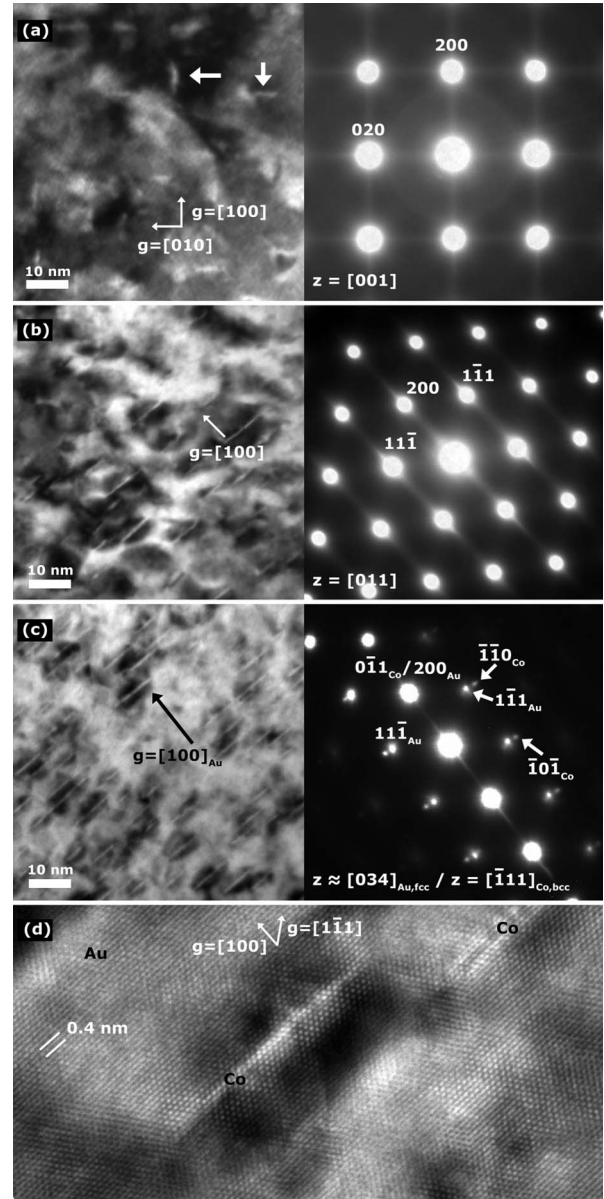


FIG. 2. TEM bright-field and HRTEM images of  $\text{Au}_{90}\text{Co}_{10}$  after isochronal annealing to 633 K with  $20 \text{ K min}^{-1}$  (cf. b in Fig. 1). (a) TEM image:  $[001]$  zone axis of the Au-rich matrix, small Co precipitates (arrows) are visible; streak formation along  $[100]$  and  $[010]$  directions in the SADP shown at the right side in (a) are due to very thin Co precipitates; extra spots due to incoherently diffracting Co precipitates are not observed. (b) TEM image:  $[011]$  zone axis of the Au-rich matrix; streak formation along  $[100]$  directions in the SADP shown at the right side in (b) [cf. (a)]; extra spots due to incoherently diffracting Co precipitates are not observed. (c) Tilted by  $9.7^\circ$  from  $[011]$  zone axis of the Au-rich matrix toward the  $[001]$  zone axis of the Au-rich matrix: streak formation along  $[100]$  directions in the SADP shown at the right side in (c) [cf. (a)]; extra spots due to the bcc crystal structure of the Co precipitate plates near the  $\{111\}$  Au-matrix spots (see arrows in the SADP) are compatible with a  $[\bar{1}11]$  zone axis for the bcc Co precipitates. (d) HRTEM image:  $[011]$  zone axis of Au-rich matrix; Co has precipitated as very thin coherent plates about 0.5–1 nm thick and 5–10 nm in width.

[001] zone axis of the Au-rich matrix two sets of mutually perpendicular precipitate plates along (100) and (010) planes of the Au-rich matrix are observed [Fig. 2(a)]; note the streaks in [100] and [010] directions in the SADP. In case of a [011] zone axis of the Au-rich matrix only one variant of the three possible precipitate plate sets can be observed in Fig. 2(b); note the pronounced contrast due to the strain field surrounding the precipitates [see also the HRTEM image shown in Fig. 2(d)].

If the electron beam is parallel to the [001] and [011] zone axes of the Au-rich matrix [Figs. 2(a) and 2(b)] the corresponding SADPs show no separate reflections which could be ascribed to the precipitates: the precipitates reveal their presence in the SADPs by streak formation along [100] and [010] (note the thinness of the platelets in these directions).

The morphology and orientation of the coherent platelets appears not compatible with the usual fcc and hcp modifications of Co. It will be demonstrated immediately below that the observations can be explained adopting a bcc modification of Co and a Bain orientation relationship of the platelets with the matrix. (i) Upon tilting the specimen by  $9.7^\circ$  from [011] toward [001], i.e., into an approximate [034] zone axis of the Au-rich matrix, small extra spots become visible next to the  $111_{\text{Au}}$  reflections in the SADP [see Fig. 2(c)]. (ii) The measured  $d$  spacing for these extra reflections is  $0.206 \pm 0.002$  nm. From (i) and (ii) it follows that these extra spots are compatible with  $\{110\}$  reflections due to the presence of bcc Co precipitates satisfying a  $[\bar{1}11]_{\text{Co,bcc}}$  zone axis (see further discussion below). This is compatible with a Bain orientation relationship between the fcc Au-rich matrix and the bcc Co precipitates:  $(100)_{\text{Au,fcc}} \parallel (100)_{\text{Co,bcc}}$  and  $[001]_{\text{Au,fcc}} \parallel [011]_{\text{Co,bcc}}$ . By performing similar tilting experiments these results could be validated: e.g., tilting into the  $[\bar{1}13]_{\text{Co,bcc}}$  zone axis, which is close to the  $[012]_{\text{Au,fcc}}$  zone axis, clear evidence for the  $1\bar{2}1$  and  $2\bar{1}1_{\text{Co,bcc}}$  diffraction spots at the appropriate locations in the SADP was obtained.

A HRTEM image, for the case of an [011] zone axis of the Au-rich matrix is shown in the Fig. 2(d). The Co precipitate plates, two to three atomic layers thick and 5–10 nm long, exhibit a coherent interface along  $\{100\}$  lattice planes of the surrounding Au-rich matrix. A platelike morphology as revealed for the precipitates developing in the initial stage of precipitation has been observed before but the crystal structure of the precipitate was not investigated<sup>23,24</sup> or was assumed to be fcc.<sup>25</sup>

TEM bright-field and HRTEM images and the corresponding SADP, taken after isochronal annealing up to 668 K with  $20 \text{ K min}^{-1}$  [corresponding with the shoulder at the high-temperature side of the main exothermic peak (Fig. 1 top) and hardness decrease after peak hardness (Fig. 1 bottom)] are shown in Fig. 3. As compared to the stage of peak hardness with bcc Co precipitates, coarsening of the platelike precipitates has occurred. Some precipitates show locally a Moiré-pattern contrast indicating a loss of coherency. The diffraction pattern ( $[\bar{1}12]$  zone axis of the Au matrix) shows spots consistent with the occurrence of the fcc structure for the Co precipitates ( $a=0.354$  nm) in accordance with a  $(110)_{\text{Au,fcc}} \parallel (110)_{\text{Co,fcc}}$ ,  $[\bar{1}12]_{\text{Au,fcc}} \parallel [\bar{1}12]_{\text{Co,fcc}}$  (cube-on-cube) epitaxial orientation relationship between

the fcc Au matrix and the (now) fcc Co precipitates. The HRTEM image presented in Fig. 3(b) ([011] zone axis of the Au matrix) shows a Co plate which has just started to bulge out in the begin of the process of transformation of bcc Co precipitate plate to fcc, more or less equiaxed Co precipitate.

A TEM image of  $\text{Au}_{90}\text{Co}_{10}$  and the corresponding SADP, taken after isochronal heating to 773 K with  $20 \text{ K min}^{-1}$  (stage “d” in Fig. 1) are shown in Fig. 4. Bulky, more or less equiaxed Co precipitates are revealed by the locations of distinct Moiré-pattern contrast as a result of the presence of double diffraction spots near “000” [see diffraction pattern in Fig. 4(a)]. A cube-on-cube, epitaxial orientation relationship between the fcc Co precipitate and the fcc Au matrix is fully compatible with the position of the reflections of Au and Co in the diffraction pattern. The residual Co concentration in the depleted Au matrix at this stage, as measured with EDX, is about 0.7 at. %, in good agreement with the published phase diagram.<sup>4</sup> Hence, the precipitation reaction has been completed at this stage.

#### IV. DISCUSSION

The here presented observations on the initial platelike precipitates are fully consistent with a bcc crystal structure for the initial Co precipitates with a lattice parameter  $a_{\text{Co,bcc}} = 0.288 \pm 0.003$  nm [derived from the measured lattice spacing for the  $011_{\text{Co,bcc}}$  reflections (see above) and confirmed by tilting experiments, e.g., tilting to the  $[\bar{1}13]$  zone axis of Co]. This equals the value of  $a_{\text{Co,bcc}} = 0.288 \pm 0.001$  nm for Co found in artificial Co/Au layer structures (cf. Refs. 19 and 20). Further, the theoretical  $d$  spacing for bcc-Co  $\{110\}$  is 0.204 nm, which is in agreement with the value found in this work.

A Bain-type orientation relationship<sup>26</sup> exists between the bcc Co precipitates and the fcc Au-rich matrix (with lattice parameter  $a_{\text{Au,fcc}} = 0.408$  nm). The habit plane is  $(100)_{\text{Au,fcc}} \parallel (100)_{\text{Co,bcc}}$  (three variants). The above crystallographic data strongly suggest that the bcc Co precipitates are coherent with the Au-rich matrix, at least along the habit plane: the value of  $a_{\text{Co,bcc}} \cdot \sqrt{2}$  closely resembles the value of  $a_{\text{Au,fcc}}$ . Hence, along the  $\{100\}_{\text{Au,fcc}}$  habit planes no significant lattice mismatch between bcc Co and fcc Au occurs. However, perpendicular to the habit planes a mismatch of  $|a_{\text{Co,bcc}} - a_{\text{Au,fcc}}| / a_{\text{Au,fcc}} \cdot 100\% = 29\%$  occurs.<sup>27</sup>

On this basis, as a consequence of the bcc crystal structure of the initial precipitates, the occurrence of the platelike morphology can be understood. The absence of separate diffraction spots originating from the bcc Co precipitates in the SADPs with  $\langle 001 \rangle$ -type zone axes of the Au-rich matrix and the presence of streaks in the SADPs (see Fig. 2) indicates that the Co plates are diffracting coherently with the Au-rich matrix (distorted by misfit strain in the plate-normal direction); see discussion for the case of platelike VN precipitates in an  $\alpha$ -Fe matrix in Ref. 29. Three sets of bcc Co plates occur in the Au-rich matrix according to the determined orientation relationship: Two sets  $\{(100)_{\text{Au,fcc}} \parallel (100)_{\text{Co,bcc}}$ ,  $[001]_{\text{Au,fcc}} \parallel [011]_{\text{Co,bcc}}$  and  $(010)_{\text{Au,fcc}} \parallel (100)_{\text{Co,bcc}}$ ,  $[001]_{\text{Au,fcc}} \parallel [011]_{\text{Co,bcc}}\}$  are visible in Fig. 2(a) (electron-beam direction  $z = [001]_{\text{Au,fcc}}$ ); the third variant



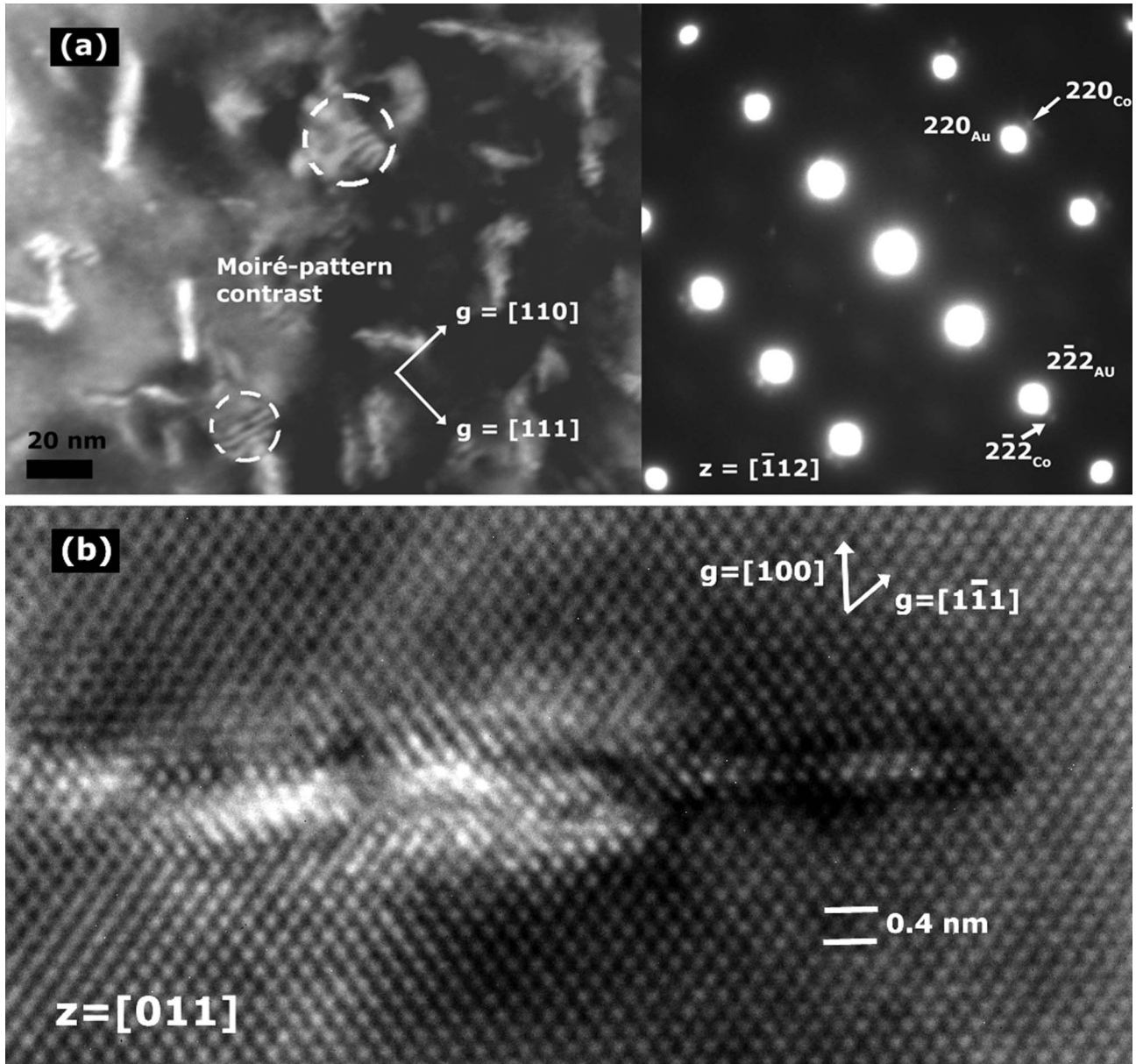


FIG. 3. (a) TEM bright-field and (b) HRTEM images of  $\text{Au}_{90}\text{Co}_{10}$  showing the precipitate morphology after isochronal annealing to 668 K with  $20 \text{ K min}^{-1}$  (cf. c in Fig. 1). (a) TEM image:  $[\bar{1}12]$  zone axis of the Au matrix; the diffraction pattern shows very intensive spots of fcc Au and weak spots of fcc Co. Some of the platelike Co precipitates show a Moiré-pattern contrast as well, indicating the beginning stage of the bcc to fcc transformation. (b) HRTEM image:  $[011]$  zone axis of the Au matrix showing the bulging of a Co plate revealing the beginning stage of the bcc-to-fcc transformation.

$\{(100)_{\text{Au},\text{fcc}} \parallel (110)_{\text{Co},\text{bcc}} \text{ and } [001]_{\text{Au},\text{fcc}} \parallel [001]_{\text{Co},\text{bcc}}\}$  concerns plates parallel to the TEM foil surface and is out of contrast because of the coherent nature of the plate/matrix interface. Also the tilting experiment shown in Fig. 2(c) validates the bcc crystal structure for the initial Co precipitates. Additional diffraction spots appear which can be indexed as  $\{011\}_{\text{Co},\text{bcc}}$ , in association with the  $[\bar{1}11]$  zone axis of bcc Co, expected for one of the above indicated three sets of precipitates after such tilting.

The natural formation of bcc Co, as in the course of precipitation process in a supersaturated solid solution, has not been reported before. Instead, in case of manmade multilayer/sandwich structures, Co layers could appear in

bcc (Refs. 17–19) or body-centered-tetragonal<sup>20,21</sup> modifications, likely as consequence of the misfit strains imposed at the layer/layer and layer/substrate interfaces in these structures.

During the DSC measurements a small shoulder at the high-temperature side of the exothermic main peak appeared at about  $T=668 \text{ K}$  (Fig. 1). The accompanying microstructural TEM investigation (Fig. 3) indicates that this shoulder can be associated with the occurrence of a bcc  $\rightarrow$  fcc transformation of the Co precipitates. The equiaxed fcc Co particles start to develop from the initial bcc Co plates; no indication for a separate (fcc Co particle) nucleation process was obtained [Fig. 3(a)].

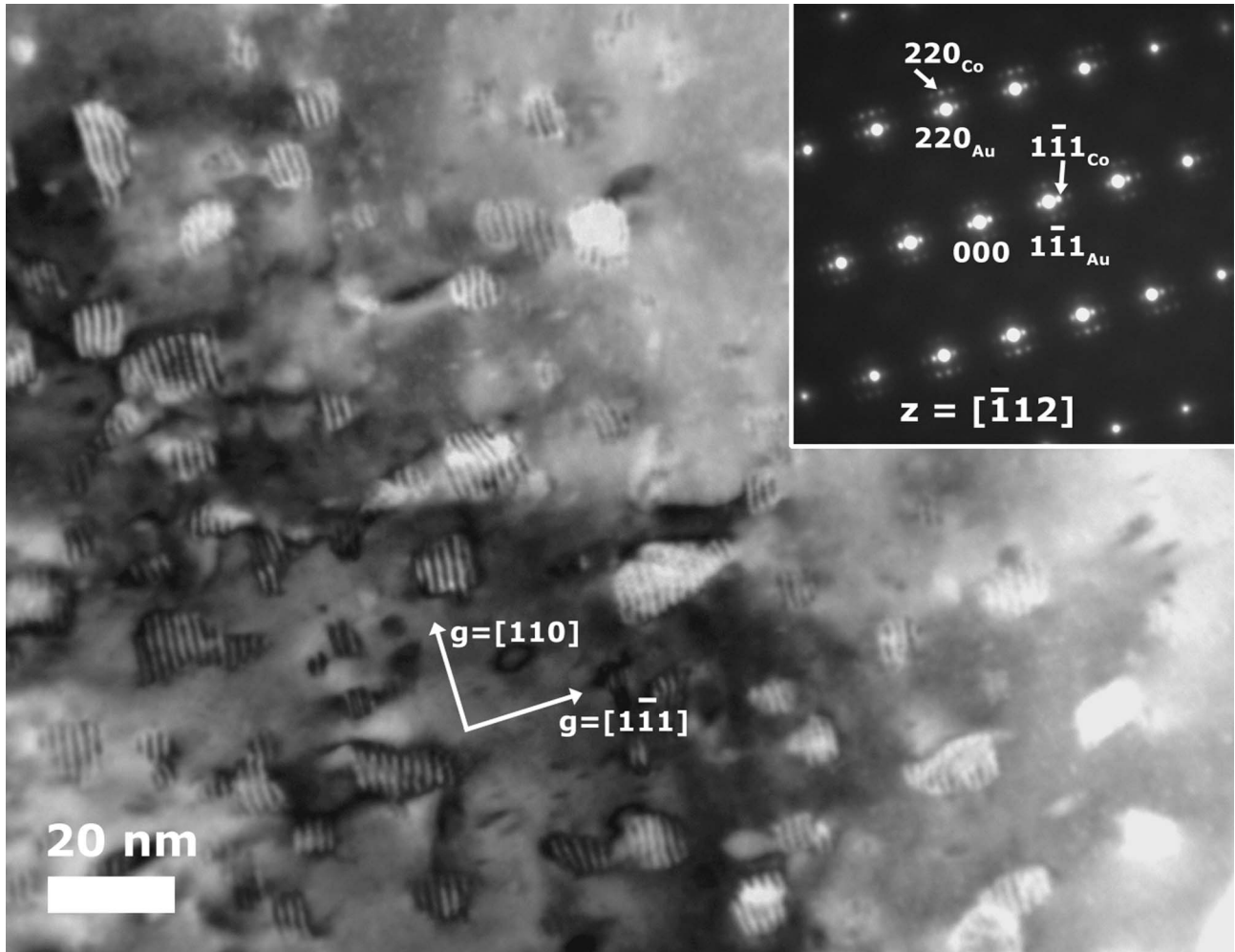


FIG. 4. TEM bright-field image ( $[\bar{1}12]$  zone axis of the Au matrix) showing the Co precipitates in  $\text{Au}_{90}\text{Co}_{10}$  after isochronal heating to 773 K with  $20 \text{ K min}^{-1}$  (cf. d in Fig. 1). Moiré fringes caused by double diffraction crossing the equiaxed fcc Co precipitates can be seen. The diffraction pattern (top right) reveals the cube-to-cube epitaxial orientation relationship between the fcc Au matrix and the from bcc-to-fcc transformed Co precipitates. Extra spots visible around 000 in the SADP are caused by double diffraction and are responsible for the Moiré-pattern contrast in the bright-field image.

Such local crystal-structure transformation, i.e., without long-range diffusion of Co as would occur in a process of dissolution (of bcc Co) and reprecipitation (of fcc Co), can be realized in the present case by a Bain transformation<sup>30</sup> from bcc to fcc Co. This transformation involves contracting two axes within the habit plane {e.g., the axes along the  $[011]$  and  $[01\bar{1}]$  directions in the  $(100)$  habit plane} and elongating a third axis perpendicular to the habit plane {i.e., the axis along the  $[100]$  direction perpendicular to the  $(100)$  habit plane}. As a consequence the here observed cube-on-cube orientation relationship is established.

After the transformation the fcc modification of the Co phase is preserved down to room temperature. The expected hcp Co phase, being stable below 695 K, was not observed in the  $\text{Au}_{90}\text{Co}_{10}$  alloy investigated. This may reflect the very small difference in bulk energy of the fcc and hcp modifications.<sup>31</sup>

The initial formation of bcc instead of fcc Co is a result of the delicate interplay, upon Co precipitation, of the Gibbs chemical energy released per unit volume precipitate and the

Gibbs interface energy absorbed per unit area precipitate/matrix interface. The Gibbs chemical energy released upon precipitation of one unit volume precipitate is larger for the fcc modification than for the metastable bcc modification. However, the Gibbs interface energy per unit area interface is smaller for the coherent bcc precipitates than for the incoherent fcc precipitates. The high supersaturation, i.e., the high driving force for cobalt precipitation, in supersaturated  $\text{Au}_{90}\text{Co}_{10}$  and the relatively low diffusivity of Co in the Au-rich matrix at the precipitation temperature, lead to the formation of many small precipitates and thus a high interface density (see Fig. 2). As a consequence, the bcc modification can be (thermodynamically) favored over the more stable fcc modification. This can be illustrated by the following estimate.

The chemical Gibbs energies released upon precipitation of bcc Co and fcc Co, in a Au 10 at. % Co alloy at 633 K, can be assessed using the data given in Refs. 32 and 33. The misfit strain to be accommodated upon precipitation of Co can be estimated adopting elastic isotropy and a rigid inclusion, according to Ref. 34. The interface energy for a (coher-

ent) interface of bcc Co with the matrix and for an (incoherent) interface of fcc Co with the matrix can be crudely estimated as  $0.2 \text{ J m}^{-2}$  and  $1.0 \text{ J m}^{-2}$ , respectively. The dimensions of the Co precipitate platelets are taken as  $10 \times 10 \times 1 \text{ nm}^3$  (see Fig. 2). It then follows that the net Gibbs energy released upon precipitation of bcc Co is about two times larger than the net Gibbs energy released upon precipitation of fcc Co for the platelet dimension considered.

Upon prolonged annealing (or by increasing the temperature) growth/coarsening of the precipitate particles take place and consequently a reduction in the interface-to-volume ratio of the precipitate particles occurs. As a consequence, the Gibbs chemical energy becomes the controlling energy term and thus the transformation of the bcc to the fcc Co crystal structure is induced, albeit accompanied with an increase in the interfacial energy per unit area interface (coherent  $\rightarrow$  incoherent interface).

## V. SUMMARY

Natural formation of, according to bulk thermodynamics, metastable bcc Co, with a platelike morphology and a Bain-

type orientation relationship with the Au-rich matrix, occurs in the initial stage of precipitation of supersaturated Au—10.12 % Co alloys. The metastable bcc modification happens because the high initial interface-to-volume ratio promotes the development of precipitates of low interface energy (as holds for the bcc Co precipitates coherent with the Au-rich matrix). Upon continued annealing growth/coarsening of the precipitate particles takes place. Then, by a Bain transformation of metastable bcc Co, the fcc Co modification can be formed which then exhibits a cube-on-cube orientation relationship with the Au-rich matrix. The low interface-to-volume ratio for the precipitate phase in an advanced stage of annealing makes possible an overcompensation of an unfavorable interfacial energy (incoherent vs coherent interface) by a more favorable chemical bulk energy (fcc vs bcc modification).

## ACKNOWLEDGMENTS

The authors are grateful to W.-D. Lang for the TEM preparation, P. Kopold for assistance with HRTEM, and to W. Sigle for the STEM analysis (all at the Max Planck Institute for Metals Research).

\*Corresponding author.

- <sup>1</sup>J. Bernardi, A. Hütten, S. Friedrichs, C. E. Echer, and G. Thomas, *Phys. Status Solidi A* **147**, 165 (1995).
- <sup>2</sup>A. Hütten, J. Bernardi, S. Friedrichs, G. Thomas, and L. Balcells, *Scr. Metall. Mater.* **33**, 1647 (1995).
- <sup>3</sup>J. Bernardi, A. Hütten, and G. Thomas, *J. Magn. Magn. Mater.* **157-158**, 153 (1996).
- <sup>4</sup>ASM International, Materials Park, Ohio 44073 (1996).
- <sup>5</sup>H. Hesemann, Ph.D. thesis, University of Stuttgart, 2002.
- <sup>6</sup>F. Sebilliau and H. Bibring, *The Mechanism of Phase Transformation in Metals* (Institute of Metals, London, 1956).
- <sup>7</sup>J. E. Bidaux, R. Schaller, and W. Benoit, *J. Phys. Colloq.* **46**, 601 (1985).
- <sup>8</sup>G. D. Hibbard, G. Palumbo, K. T. Aust, and U. Erb, *Philos. Mag.* **86**, 125 (2006).
- <sup>9</sup>J. Y. Huang, Y. K. Wu, H. Q. Ye, and K. Lu, *Nanostruct. Mater.* **6**, 723 (1995).
- <sup>10</sup>E. A. Owen and D. M. Jones, *Proc. Phys. Soc. London, Sect. B* **67**, 456 (1954).
- <sup>11</sup>H. Sato, O. Kitakami, T. Sakurai, Y. Shimada, Y. Otani, and K. Fukamichi, *J. Appl. Phys.* **81**, 1858 (1997).
- <sup>12</sup>J. Sort, J. Nogues, S. Surinach, and M. D. Baro, *Philos. Mag.* **83**, 439 (2003).
- <sup>13</sup>B. Strauss, F. Frey, W. Petry, J. Trampenau, K. Nicolaus, S. M. Shapiro, and J. Bossy, *Phys. Rev. B* **54**, 6035 (1996).
- <sup>14</sup>P. Tolédano, G. Krexner, M. Prem, H.-P. Weber, and V. P. Dmitriev, *Phys. Rev. B* **64**, 144104 (2001).
- <sup>15</sup>J. C. Zhao and M. R. Notis, *Scr. Metall. Mater.* **32**, 1671 (1995).
- <sup>16</sup>A. R. Troiano and J. L. Tokich, *Trans. Am. Inst. Min., Metall. Pet. Eng.* **175**, 728 (1948).
- <sup>17</sup>G. A. Prinz, *Phys. Rev. Lett.* **54**, 1051 (1985).
- <sup>18</sup>J. Dekoster, E. Jedryka, C. Meny, and G. Langouche, *J. Magn. Magn. Mater.* **121**, 69 (1993).
- <sup>19</sup>L. J. Wu, K. Shintaku, T. Shinjo, and N. Nakayama, *J. Phys.: Condens. Matter* **5**, 6515 (1993).
- <sup>20</sup>S. K. Kim, C. Petersen, F. Jona, and P. M. Marcus, *Phys. Rev. B* **54**, 2184 (1996).
- <sup>21</sup>N. Spiridis, T. Slezak, M. Zajac, and J. Korecki, *Surf. Sci.* **566-568**, 272 (2004).
- <sup>22</sup>G. W. H. Höhne, W. F. Hemminger, and H.-J. Flammersheim, *Differential Scanning Calorimetry*, 2nd ed. (Springer-Verlag, Berlin, 2003).
- <sup>23</sup>C. G. Lee, S. H. Kim, D. H. Lee, and K. Fukamichi, *IEEE Trans. Magn.* **35**, 2856 (1999).
- <sup>24</sup>V. Y. Zenou, G. Kusinski, L. Yue, and G. Thomas, *J. Mater. Sci.* **38**, 2679 (2003).
- <sup>25</sup>N. Kataoka, H. Takeda, J. Echigoya, K. Fukamichi, E. Aoyagi, Y. Shimada, H. Okuda, K. Osamura, M. Furusaka, and T. Goto, *J. Magn. Magn. Mater.* **140-144**, 621 (1995).
- <sup>26</sup>E. C. Bain, *Trans. Metall. Soc. AIME* **70**, 25 (1924).
- <sup>27</sup>Within the experimental accuracy (e.g., the measured spacing for  $\{110\}_{\text{Co,bcc}}$  equals  $0.206 \pm 0.002 \text{ nm}$ , whereas a value of  $0.204 \text{ nm}$  is expected for bcc Co with  $a=0.288 \text{ nm}$ ) only a very small tetragonal distortion might be possible. Theoretical calculations suggest that the bcc modification of bulk Co cannot be truly metastable (Ref. 28). For an explanation of the (meta)stability of the tiny bcc Co platelets in a Au-rich matrix see later in this paper.
- <sup>28</sup>A. Y. Liu and J. Singh, *J. Appl. Phys.* **73**, 6189 (1993).
- <sup>29</sup>N. E. V. Vives Díaz, S. S. Hosmani, R. E. Schacherl, and E. J. Mittemeijer, *Acta Mater.* **56**, 4137 (2008).
- <sup>30</sup>J. Rifkin, *Philos. Mag. A* **49**, L31 (1984).
- <sup>31</sup>A. Fernández Guillermet, *Int. J. Thermophys.* **8**, 481 (1987).
- <sup>32</sup>H. Okamoto, T. B. Massalski, T. Nishizawa, and M. Hasebe, *J. Phase Equilib. Diffus.* **6**, 449 (1985).
- <sup>33</sup>A. T. Dinsdale, *CALPHAD: Comput. Coupling Phase Diagrams Thermochem.* **15**, 317 (1991).
- <sup>34</sup>J. D. Eshelby, *Proc. R. Soc. London, Ser. A* **241**, 376 (1957).